Chemistry–A European Journal
Research Article
doi.org/10.1002/chem.202403129
Chemistry Europe
European Chemical Societies Publishing
www.chemeurj.org

Seeing Double: The Persistent Dimer-of-Dimers Structure of Drug Resistant Influenza A M2

Marianna Stampolaki,[a] Abel Cherian Varkey,[a] Evgeny Nimerovsky,[a] Andrei Leonov,[a] Stefan Becker,[a] and Loren B. Andreas*[a]

The currently circulating S31N variant of the M2 proton channel of influenza A is resistant to antiviral drugs. Recently, there has been a growing concern regarding the impact of the lipid environment on the structural features of the S31N variant. The native symmetry of the M2 tetramer remains controversial. Here we show that S31N M2 persists in a dimer-of-dimers structure in different lipid preparations independent of the amount of solvating lipids up to at least 180 lipids per tetramer. NMR spectra clearly detect the characteristic resonances of the dimer-of-dimers of M2 (residues 18–60 or 18–62) reconstituted in lipids. NMR-based distance measurements indicate that two isoleucine residues with upfield shifted alpha carbon resonances, typical of extended conformations, are compatible with a particular side-chain rotameric state and helical backbone geometry. These chemical shifts are therefore compatible with the expected native transmembrane helical fold. Symmetry breaking at the pH sensing H37 residues, detected via peak doubling, is a stable feature of S31N M2 based on the reference strain Udorn/1972(H3N2). By contrast, the spectrum is dramatically altered for Columbia/2014/(H3N2) M2, which differs in sequence in the amphipathic helices. This highlights an allosteric coupling between the amphipathic helices and the pH sensing residues.

Introduction

The structure of small helical membrane proteins is influenced by environmental conditions.[1] This is especially true for oligomeric viral membrane proteins, since the complex is held together by relatively weak interactions, primarily van der Waals interactions, with polar or occasionally ionic interactions found at the core of the assembly within the membrane.[2] By contrast, β-barrel membrane proteins, as well as many soluble proteins, assemble with many strong hydrogen bonding interactions stabilizing the tertiary structure of the protein backbone.[3] The Influenza A M2 protein demonstrates this environmental sensitivity: Figure 1 shows selected structures of wild type (WT) and S31N M2, which were determined from preparations using different membrane mimetics, including both detergent and lipid. A substantial range of helix tilt angles can be appreciated from these structures, which also demonstrate differences in the conformations of the important pH sensing histidine residues,[4] the gating tryptophan,[5] and for S31N M2, the asparagine that confers resistance to the drugs rimantadine and amantadine.[6]

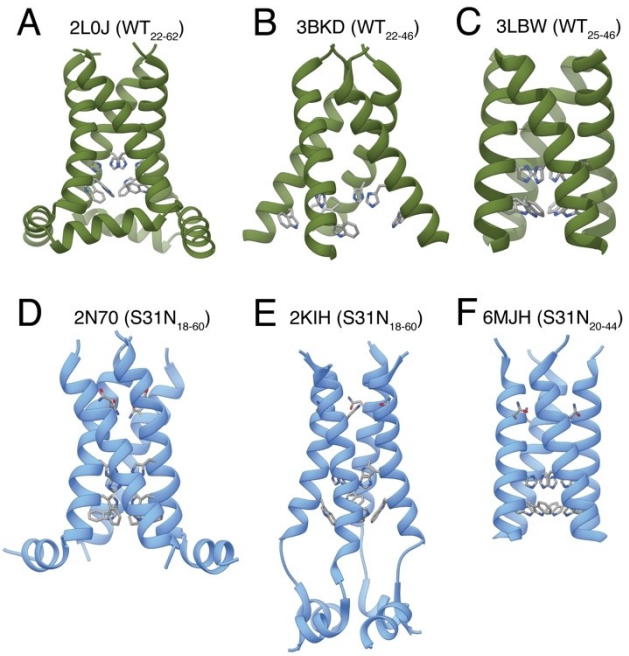

Figure 1. Representation of selected WT (green) and S31N (blue) structures, some of which include the amphipathic helices. Structure A, D, E derive from NMR data, and B, C, F from X-ray crystallography. Different packing of the TM domain and amphipathic helices occurs in each M2 structure depending on the lipid or detergent reconstitution or crystallization conditions. The conformation of the pore residues also varies: H37, W41, and N31 residues are shown as sticks. Note that the WT sequence refers to the Udorn/1972(H3N2) strain, which has become the reference sequence for M2 studies.

Solid-state NMR is an established technique that can probe the structure of the protein in hydrated lipid bilayers, and as such, a method suitable to probe native protein structure.[7]

[a] M. Stampolaki, A. Cherian Varkey, E. Nimerovsky, A. Leonov, S. Becker, L. B. Andreas
Department of NMR Based Structural Biology, Max Planck Institute for Multidisciplinary Sciences, Am Fassberg 11 Göttingen, Germany
E-mail: land@mpinat.mpg.de

Supporting information for this article is available on the WWW under https://doi.org/10.1002/chem.202403129

Indeed, it is well known that the lipid environment can be crucial for obtaining the biologically relevant structure of the protein.[7a,d,8] In oriented samples (OS), the spectrum is exquisitely sensitive to small changes in the tilt angle of alpha helices.[9] For membrane proteins, the sample is typically oriented by assembling the bilayers together with a stack of thin glass slides such that a single axis of alignment is achieved. Using magic-angle spinning (MAS) NMR, the effects of different lipids[10] as well as drug binding can be investigated via chemical shift perturbation without the requirement for sample alignment.[11]

The M2 protein is of medicinal and biological interest since it is responsible for essential viral function, in particular, its activity as a proton channel[12] and its role in viral budding.[13] The drugs amantadine and rimantadine block the proton channel activity of the protein by binding to the pore of the protein near residues 27–34.[14] Amphipathic helix residues, approximately residues 47–60, have been shown to influence membrane curvature during budding.[15] C-terminal to residue 60, the cytoplasmic tail of M2 has been shown to be important in virus assembly, with residues 71–76 of the cytoplasmic tail in particular interacting with the viral protein M1.[16]

Thus, a peptide comprising residues of the transmembrane and amphipathic helices emerged as a minimalistic protein sequence to study the channel function of M2. This peptide, dubbed the conductance domain (CD), demonstrated conduction rates and drug inhibition indistinguishable from the full-length protein, when studied in oocytes or lipid bilayers.[17] It was subsequently utilized for solid-state NMR structure determination via OS[18] and MAS[19] NMR. The conductance domain structure has not been captured via crystallography, with the exception of a V27A mutant that demonstrated an extended helix in the crystal.[20] Slightly shorter peptides have been successfully crystallized from a variety of conditions, including impressive structures solved from lipidic cubic phase in which the structure of pore-lining water molecules was revealed.[21]

Despite similarities in the lipid bilayer preparations, the solid-state NMR structures of conductance domain M2 show marked differences. A structure determined from OS NMR is four-fold symmetric at the backbone, with symmetry broken only at the side chain of H37 residues, which form two pairs of imidazole-imidazolium dimers.[18] By contrast, a structure determined using magic-angle spinning NMR detected a dimer-of-dimers symmetry not only at H37 side chains, but also at the backbone of transmembrane residues.[19]

There are several possible explanations for these differences, including differing sensitivities of MAS NMR and OS NMR to symmetry breaking. For example, while exquisitely sensitive to changes in orientation of the helices, OS NMR spectra are insensitive to translations of the helix in the bilayer, as well as rotations about the bilayer normal. There were also differences in the lipid composition between the two studies, as well as the exact length of the protein construct, either residues 18–60 or 22–62.

Cross and coworkers reported that the difference in structures is caused by an insufficient amount of lipids in MAS NMR preparations.[22] The dimer of dimers structure of S31N $M2_{18–60}$ was determined from samples assembled with a lipid to protein tetramer ratio (LPR_T) of 28. Two sets of peaks are evident in MAS NMR spectra under these conditions, due to the two-fold symmetry of the dimer-of-dimers. On the other hand, Cross and coworkers identified a single set of resonances when the protein was reconstituted with an LPR_T of 120, and concluded that the tetramer is 4-fold symmetric. Cross and coworkers also pointed out that there are two anomalous isoleucine resonances in the MAS NMR spectra of S31N M2 at an LPR_T of 28, which they describe as occurring in a 'non-helical Cα chemical shift range for Ile'.[22]

In order to address the above discrepancy in reported CD M2 assemblies in lipid bilayer preparations, here we use MAS NMR as a sensitive probe of protein structure to investigate the influence of lipids, lipid concentration, protein sequence length, and amphipathic helix variants. We additionally investigate the structural underpinnings of the unusual isoleucine chemical shifts, which are in fact compatible with helical secondary structure.

Results and Discussion

Spectra of S31N $M2_{18–60}$ in Different Lipids or Sample Preparation Protocols

Starting with S31N $M2_{18–60}$, we recorded multidimensional MAS NMR spectra to track potential changes in the chemical shifts that can be induced by the presence of different concentration or type of lipid. Figure 2 superimposes spectra reconstituted under varying conditions. The signals are well dispersed in the Cα-N projection of the 3D (H)CαNH spectra, such that the unusual Ile resonances are fully resolved. Comparison of the (H)NH spectra of these samples is shown in Figure S1. The spectrum is stable across the investigated parameter space, with only minor changes in peak positions observed. Figure 2A compares a lipid to protein tetramer ratio (LPR_T) of 28 with 180 in 1,2-diphytanoyl-sn-glycero-3-phosphocholine (DPhPC) lipid. Figure 2B compares the spectrum in DPhPC with a mixture of 1,2-dioleoyl-sn-glycero-3-phosphocholine (DOPC) and 1,2-dioleoyl-sn-glycero-3-phosphoethanolamine (DOPE) lipids at an LPR_T of 180. These lipids were chosen to match the composition reported by Cross and coworkers,[22,23] and the LPR_T of 180 was chosen to exceed the value of 120 reported in their work. Reconstitution via detergent dialysis results in fully hydrated bilayers,[24] with a water to lipid molar ratio of about 95 (Figure S5).

To rule out the potential impact of the use of different reconstitution protocols on the protein folding and consequently on its spectroscopic behavior, we performed two lipid reconstitution protocols. Figure S2A compares our reconstitution protocol with the protocol of Cross and coworkers, using LPR_T of 180 or 120. Figure S2D–G shows each spectrum separately. Our protocol involves solubilization of all components in octyl glucoside detergent followed by dialysis to remove detergent. The protocol of Cross and

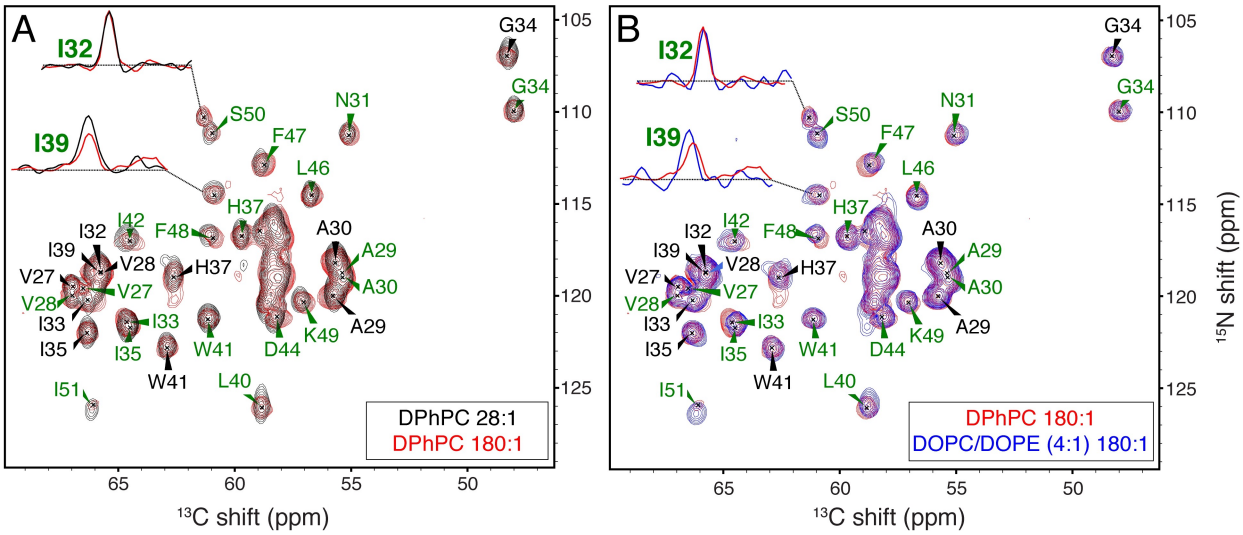

Figure 2. Spectroscopic comparison of ^{13}C,^{15}N S31N $M2_{18–60}$ reconstituted at high and low LPR_T. ^{15}N-$^{13}C_\alpha$ projections of the (H)C_αNH spectra of the protein reconstituted in A) DPhPC at an LPR_T of 28 : 1 (black) or 180 : 1 (red) and B) DPhPC (red) or DOPC/DOPE (4 : 1) (blue) at an LPR_T of 180 : 1. Spectra were recorded on an 800 MHz Bruker spectrometer with a 3-channel 1.3 mm probe at 55 kHz MAS. 1D slices of I32 and I39 peaks are shown.

coworkers instead involves dissolving the lipids and M2 in organic solvent, followed by removal of solvent to form a lipidic film. The sample is then hydrated via incubation in the presence of buffer. It is evident from the superimposed ^{15}N-^{1}H correlation spectra that there is no significant change in the resonances.

Note that there are also differences in the preparation protocols prior to reconstitution. For example, we use HPLC purification following chemical cleavage from a fusion protein, while Cross and coworkers precipitated the protein in trichloroacetic acid following enzymatic cleavage from a fusion protein. Although we have not ruled out the influence of the protein purification protocol, we expect that the detergent or organic solvent conditions are sufficiently disaggregating such that the history of the sample prior to reconstitution does not impact the final fold. The protein in detergent showed a single set of peaks,[25] suggesting that the dimer of dimers structure emerges during reconstitution in lipids.

There is a general concern in the research of membrane proteins regarding how closely it is possible to approach the native state(s) of a protein by emulating the specific physical and chemical properties of the native environment. Solid-state NMR provides access to the structure of membrane proteins within defined lipid compositions that fulfill the main requirement of membrane proteins by reproducing many characteristics of the native membrane.[7c,26] Still, membrane protein structures have been shown to respond to the detailed lipid composition,[10] emphasizing that the specific nature of the lipids can be important. Numerous studies have confirmed how different conditions in the membrane environment, such as using detergents to mimic lipids, can impact the tertiary structure, flexibility, dynamics, or functional states of membrane proteins.[7a,d] These effects are directly reflected in NMR spectra, primarily in the form of chemical shift perturbation or in changes in peak intensity and linewidth. Inversely, changes in the spectrum offer a direct, site-specific readout of structural and dynamical change.

Here our interest lies in the drug resistant S31N M2 variant, which is prevalent in circulating influenza A strains.[6a] We previously reported a MAS-NMR-based structure of S31N M2CD consisting of residues 18–60. We found that the protein adopts a dimer of dimers structure in lipid bilayers, and thus imposed C2 rather than C4 symmetry during the structure calculation.[27] We later learned that an H37-H37 hydrogen bond is central to the breaking of symmetry.[28] Symmetry breaking was not detected by oriented sample NMR, leading to a largely symmetric structure determination based on oriented sample NMR data. The spectra of Figures 2 and 3 clearly indicate the presence of a dimer-of-dimers across different sequence lengths, and for both high and low LPR.

Since the MAS NMR samples were previously prepared with minimal lipids, one possible explanation for the apparent discrepancy was a putative transition between two-fold and four-fold symmetric tetramers, which would be influenced by the amount of solvating lipid. Cross and coworkers recently argued that this is the case, and that the more dilute conditions represent the native conformation.[22] Specifically, the M2 structure was reported to be sensitive not only to the membrane composition, but to the lipid-to-protein tetramer ratio (LPR_T), with a high ratio of at least 120 reported to result in a highly symmetric tetramer, and a lower LPR reported to result in a dimer of dimers structure. The central evidence put forward by Cross and coworkers was that the I32 and I39 peaks characteristic of the dimer-of-dimers spectrum were not detected in a ^{13}C-^{13}C 2D spectrum of the protein at LPR_T of 120. However, they presented no comparative data at lower LPR, conditions under which such peaks should certainly have been detectable. Since the ^{13}C-^{13}C correlation spectrum of the six isoleucine resonances is highly degenerate, a main Cα-Cβ peak

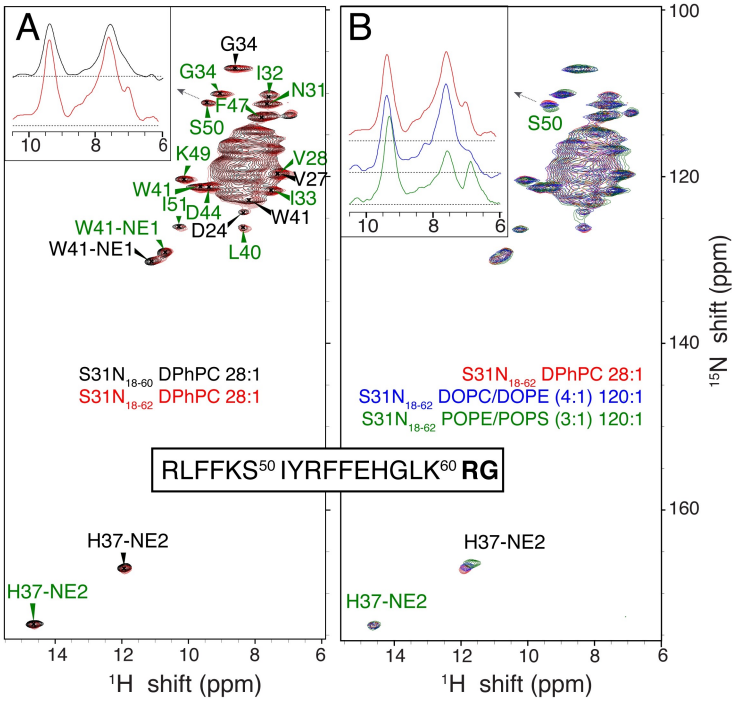

Figure 3. Spectroscopic comparison of different ^{15}N S31N M2 constructs in different lipid environments. (H)NH spectra of A) S31N $M2_{18–60}$ (black) and S31N $M2_{18–62}$ (red) in DPhPC at an LPR_T of 28:1, B) S31N $M2_{18–62}$ in DPhPC (red) at an LPR_T of 28:1, and in DOPC/DOPE (4:1) (blue) or POPE/POPS (3:1) (green) at an LPR_T of 120:1. Spectra were recorded on a 1.2 GHz Bruker spectrometer with a 3-channel 1.3 mm probe at 55 kHz MAS. The sequence of the amphipathic helix of S31N M2 (starting at residue 45) is shown in the box. Slices are shown at the position of the S50 peak.

is observed in the spectrum presented by Cross and coworkers, as well as a smaller peak assigned by them as I51.

We recorded a comparable 2D spectrum at the same magnetic field of 600 MHz and in a higher magnetic field of 1.2 GHz (Figure S4). These spectra both show spectral crowding of isoleucine cross-peaks with 6 out of 11 resonances contributing to an unresolved Cα-Cβ peak, and 3 more contributing to the smaller peak labeled as I51 by Cross and coworkers. By contrast, the unusual isoleucine resonances, I32 and I39, do not overlap with other peaks and therefore can be expected to contribute about 3-fold less signal. Indeed, in a 2D ^{13}C-^{13}C correlation spectrum (Figure S4), the I32 peak is about 4-fold less intense. We can therefore speculate that the unusual I32 and I39 resonances are therefore not detected in the spectrum presented by Cross and coworkers because of the challenge of detecting the weaker peaks. The resolution of the spectrum substantially improves at the higher magnetic field of 1200 MHz (Figure S4A).[29] However, the Ile carbon resonances are highly degenerate, leading to peak overlap even at 1200 MHz.

Having examined the above different lipid reconstitution conditions and having observed little to no impact on the M2CD spectra, we considered whether changes in the M2CD construct, specifically in the amphipathic helices, could influence the spectrum. The construct of Cross and coworkers contains an additional two residues towards the end of the amphipathic helix, residues 61 and 62. Figure 3A compares the spectrum of $M2_{18–60}$ and $M2_{18–62}$ in DPhPC lipids at 28:1 LPR_T. The ^{15}N-^{1}H correlation spectra of the two samples are almost perfectly overlaid. Figure 3B compares $M2_{18–62}$ in different lipid compositions and LPR_T of 28 or 120, including the DOPC/DOPE mixture used by Cross and coworkers.[22,23] Since the viral membrane composition contains a substantial amount of negatively charged lipids,[30] we also reconstituted $M2_{18–62}$ in a mixture of POPE and POPS (Figure 3B). The spectra of S31N $M2_{18–62}$ are almost identical in all lipid compositions tested. The only notable chemical shift changes were those of one of the H37 side chains and S50 in POPE/POPS (3:2), which were $<$0.2 ppm in ^{1}H and ~0.8 ppm in ^{15}N. The change at H37, which lies at the heart of the M2 tetramer, appears to be an indirect influence of the lipids. On the other hand, the change at S50 can be easily rationalized since it lies in the amphipathic helix, which faces the lipids. Each of the spectra is also shown separately in Figure S2.

An Allosteric Link between the Amphipathic Helices and the pH Sensing Residues

The native protein is palmitoylated at cysteine 50, a modification that is not straightforward to synthesize from protein expressed in bacteria. Structural biology studies have substituted cysteine at position 50 for serine, and therefore lack the palmitoylation of native M2. We therefore also measured the spectrum of an N31 M2 variant (Columbia/P0067/2014 H3N2) that lacks cysteine, and instead has phenylalanine at position 50 (Figure 4B and Figure S3). The spectrum of this Columbia variant in three lipid compositions does not resemble the dimer

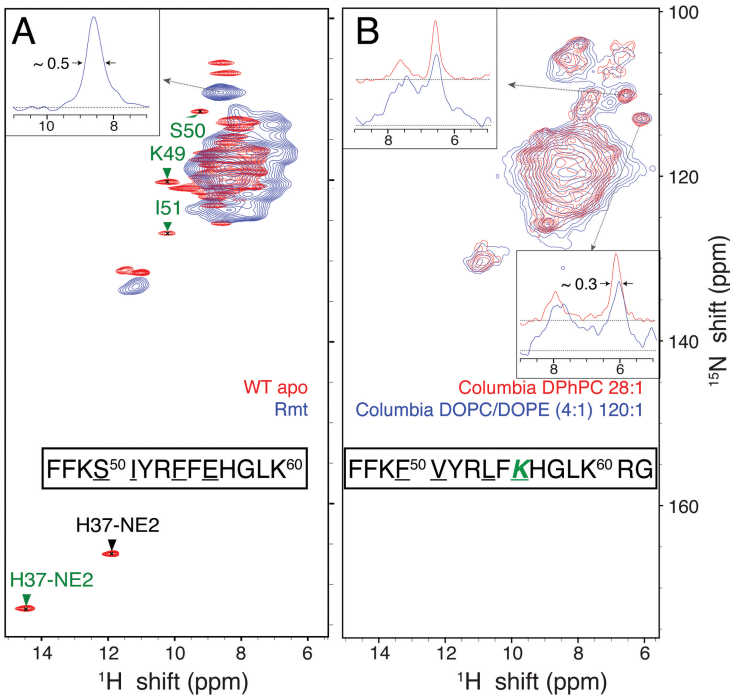

Figure 4. Spectroscopic comparison of ^{15}N, ^{13}C-labelled WT M2 bound to rimantadine[11b] and the ^{15}N-labelled Columbia M2 variant. (H)NH spectra of A) apo WT $M2_{18–60}$ (red) and rimantadine-bound WT $M2_{18–60}$ (blue) in DPhPC at an LPR_T of 28 : 1, and B) N31 Columbia $M2_{18–62}$ in DPhPC at an LPR_T of 28 : 1 (red) and in DOPC/DOPE (4 : 1) at an LPR_T of 120 : 1 (blue). Spectra were recorded on an 800 MHz (A) or 1.2 GHz Bruker (B) spectrometer with a 3-channel 1.3 mm probe at 55 kHz MAS. Slices of selected peaks are shown to show the remaining resolution. Note that 0.5 ppm at 800 MHz is comparable to 0.3 ppm at 1.2 GHz. The sequence of the amphipathic helix is shown in the boxes, starting from residue 47. Residues that are different in Columbia M2 are underlined, and an E–K substitution in the Columbia variant is shown in green.

of dimers spectrum of Udorn M2. However, the change does not appear to be specific to the substitution at position 50, since F50S Columbia also does not resemble the Udorn M2 dimer of dimers spectrum (Figure S3B). The H37-Nε2 side chain peaks are not detected in any of the Columbia variant spectra. By contrast, for WT M2 or S31N M2, the H37 side-chain peaks provided a clear signature of a stable imidazole-imidazole hydrogen bonding interaction between H37 residues.[28]

Thus far, the dimer-of-dimers structure has been reported for both WT and S31N M2 when the protein construct includes an amphipathic helix, namely the residues 18–60 of the Udorn strain.[11b,27] By contrast, crystal structures have either shown lack of symmetry, or four-fold symmetry. Here we extended the construct by two residues, in order to match the complete set of C-terminal residues implemented by Cross and coworkers. The spectrum of this 18–62 construct of M2 overlaps almost perfectly with the 18–60 spectrum, indicating that the dimer-of-dimers structure is preserved.

By contrast, the spectrum of a Columbia variant of M2, which contains amino acid substitutions in the amphipathic-helix residues, does not overlap, and notably, the H37 sidechain resonances that are emblematic of the H37-H37 hydrogen bonding, are not detected. The resonances also appear to be broadened. These features are reminiscent of spectra acquired for WT M2 in the presence of the inhibitor rimantadine.[11b] Figure 4 shows a comparison between drug bound M2 and the Columbia variant. Notably, spectra obtained with the inhibitor exhibited loss of signal from the amphipathic helix and at the same time breaking of the H37-H37 hydrogen bond and yet retained two-fold symmetry.[11b,19] Considering the results from the Columbia variant, we can therefore describe an allosteric coupling between the H37 residues and the amphipathic helix. Firstly, drug binding to the pore of the protein near G34 results in loss of signal from H37 sidechains, as well as loss of signal from the amphipathic helix. Secondly, substitution of residues in the amphipathic helix results in loss of signal from the H37 sidechains. Chemical shift perturbations due to changing the lipid composition (Figure 4B) at the H37 sidechain as well as at S50 are a further possible signature of this allosteric coupling.

Structural Origin of I32 and I39 Chemical Shifts

Having established that the spectrum, and therefore the structure of the Udorn sequence of M2 is stable across a range of sample conditions, we turned our attention towards explanation of the unusual isoleucine chemical shifts. The alpha carbons of I32 and I39 are shifted to 61.4 and 60.4, respectively, which is about 5 ppm away from the other isoleucine resonances and falls in a region of the spectrum that is typical of more extended geometries, such as beta sheet secondary structure. This is a surprising finding for residues in the middle of a transmembrane helix. To gather more information about the conformation of these residues, we recorded ^{15}N-^{13}C

correlation spectra of M2CD that reveal carbon resonances in close proximity to the backbone nitrogen. For this purpose, we used transferred rotational echo double resonance (TREDOR).[31] Figure 5A shows a representation of some of the possible rotameric states of isoleucine, together with chemical shifts of those rotamers calculated using density functional theory (DFT) and reported previously by Siemons et al.[32] In WT M2, which does not display these unusual isoleucine chemical shifts, the $C\gamma_1$ resonance of I39 is detected in the TREDOR spectrum, which is consistent with a *gauche-* χ_1 rotameric state. By contrast, the $C\gamma_2$ resonance of both I32 and I39 are detected in S31N M2, but not the $C\gamma_1$, which is consistent with a *trans* χ_1 rotameric state. In detail, the WT N–$C\gamma_1$ distance in residue I39 was found to be 2.89 ± 0.15 Å. The S31N N–$C\gamma_2$ distances in I32 and I39 were found to be 2.92 ± 0.08 Å and 3.12 ± 0.20 Å, respectively. This agrees with the expected distance of about 2.95 Å for a carbon in the *gauche* configuration with respect to the nitrogen. The 3.85 Å N–$C\gamma_1$ distance in the *trans* configuration (or the N–Cγ2 distance in *gauche-*) is near or below the detection limit. These data indicate a change in rotamer population between WT and S31N M2. Since the alpha carbon resonance is sensitive to the rotameric state in isoleucine residues,[32] these data suggest that the rotameric states are responsible for the unusual chemical shifts, as discussed below.

Both I32 and I39 occur in the transmembrane alpha helix of M2 and are flanked by residues whose chemical shifts clearly indicate helical secondary structure yet their Cα chemical shifts near 60 ppm are typical of beta sheet secondary structure. Backbone torsion angles predictions by TALOS-N[33] (Table S1) resulted in φ and ψ angles for I32 that are helical, but deviate from ideal helical φ,ψ values of about −60°, −45°. The values also depend substantially on the input chemical shift list. The

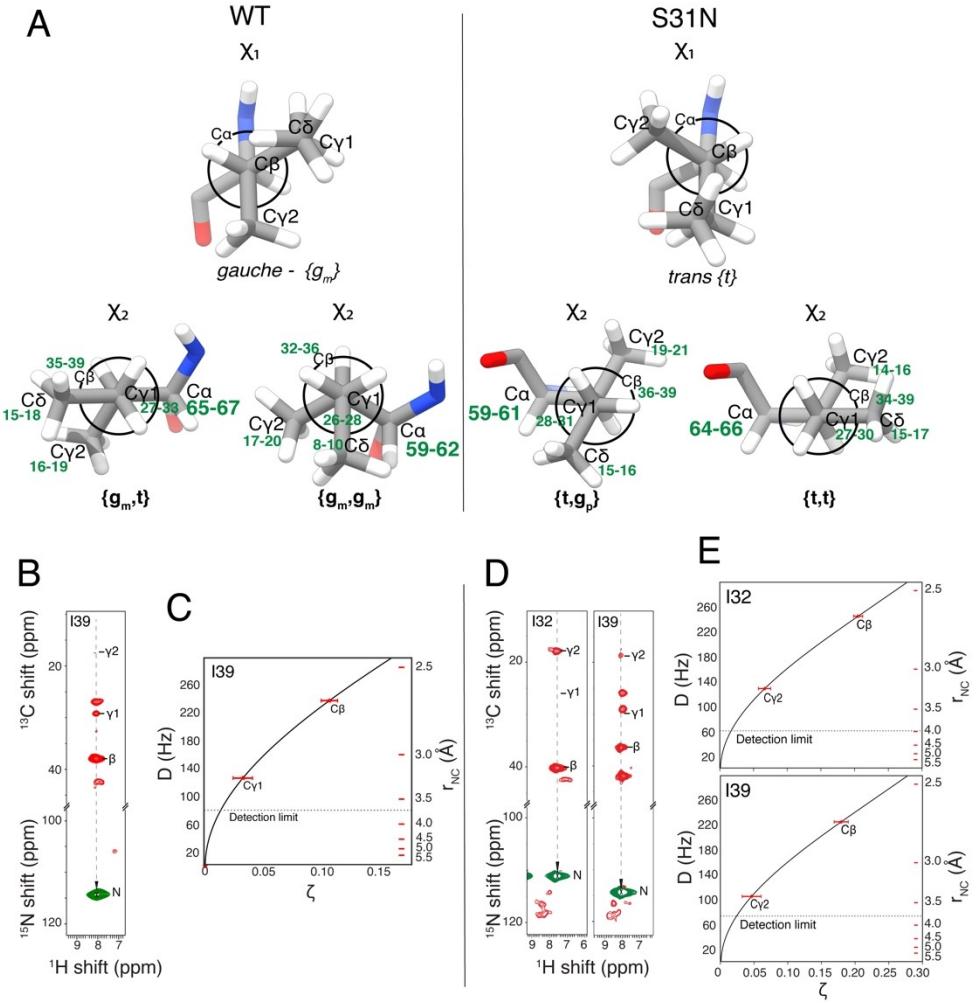

Figure 5. Rotameric states of isoleucine and TREDOR data for I32 and I39 that define the χ_1 torsion angle. A) Some of the rotameric states that are accessible to isoleucine, labeled according to their χ_1, χ_2 rotameric states: g_m = *gauche-*, g_p = *gauche+*, t = *trans*. The calculated chemical shifts reported previously in ref.[32] for the different rotamers are annotated in green. B,D) Strips from 3D 4 ms TREDOR spectra that show a short distance to the backbone nitrogen for the γ_1 carbon in the WT protein for I39, but for the γ_2 carbon in the S31N mutant for I32 and I39, indicating a change in rotamer population. DPhPC-reconstituted ^2H, ^{13}C,^{15}N-labelled S31N $M2_{18-60}$ and ^{13}C,^{15}N-labelled WT $M2_{18-60}$ were used for these experiments at LPR_T of 28. C,E) Plots of the peak intensity ratio ζ (details in the supplementary information) vs dipolar coupling strength, D, and distances, r, on the left and right y-axes, respectively. Error bars of 2σ are shown, as determined from the signal-to-noise ratios of the TREDOR peaks. An intensity ratio occurring from a peak lower than 3 times the spectrum noise level is indistinguishable from noise, and therefore falls below the detection limit, which is demarcated by the horizontal dashed line.

prediction for I39 is essentially ideal helical values for φ and ψ, despite the upfield Cα resonance. The Cα chemical shift is known to be impacted by the side-chain rotameric state since Cα is one of the central atoms that define the χ_1 angle. With a branched structure at the beta carbon, several different isoleucine sidechain rotameric states occur with similar energies, such that the rotameric state might be influenced by subtle changes in protein structure.

The dependence of the isoleucine alpha carbon chemical shift on the rotameric state has been recently reported. Siemons et al.[32] previously investigated the five Ile rotameric states: (g_m,t), (g_m,g_m), (g_p,t), (t,t), (t,g_p), that account for 97% of the total reported in a set of high-resolution crystal structures. By using density functional theory (DFT) calculations on a model peptide, they calculated the isoleucine ^{13}C chemical shift profiles as a function of the (χ_1,χ_2) angles, and found that the accessible rotameric states can account for more than 5 ppm differences in the Cα chemical shift, a similar amount as the difference between alpha and beta secondary structure. Specifically, the calculated Cα chemical shift for isoleucine in an alpha helix ranged from 59–68 ppm depending on the rotameric state.

We used these chemical shift profiles together with ^{13}C-^{15}N distance data using TREDOR to assess whether rotameric states are the most likely explanation for the unusual chemical shifts of I32 and I39. Figure 5A shows a representation of four (χ_1,χ_2) rotameric states from among the five that are likely based on crystal structures, together with the calculated shifts of Siemons et al.[32] Figure 5B shows TREDOR data of WT and S31N M2CD that are sensitive to the χ_1 angle by measuring the N to Cγ dipolar coupling. The dipolar coupling depends on the internuclear distance, and thereby helps to define the possible rotameric states. Note that rotameric states of isoleucine are typically in fast exchange, and that the NMR observables are therefore population weighted averages of multiple states. Since a single rotamer often dominates, we hereafter refer to the dominant rotameric state as simply the rotameric state. In the TREDOR spectra, transferred magnetization is detected at only one of the two Cγ atoms of I32 and I39 for both WT and S31N. Specifically, $C\gamma_1$ is detected for WT I39 and $C\gamma_2$ is detected for S31N I32 and I39. WT I32 could not be analyzed due to signal overlap. The absence of the second Cγ cross-peak implies that it is located far from the amide nitrogen, below the detection limit of the TREDOR spectrum. Thus, either the $C\gamma_1$ or $C\gamma_2$ can be deduced to be in closer proximity to the amide nitrogen, with the other *trans* to the nitrogen. As a result, the χ_1 dihedral angle ($C_{\gamma 1}C_\beta$-$C_\alpha N$), that best describes the Cγ data, is a *gauche*- (g_m) conformation for WT I32 and *trans* (t) for S31N I32 and I39 (Figure 5A). Due to the longer distances involved, we could not detect cross-peaks that are related to Cδ atoms and thus the χ_2 conformation of the two residues could not be determined from TREDOR. Hence, there are two possible (χ_1,χ_2) rotameric states for WT I39, (g_m, t) and (g_m, g_m), with (g_m, t) a better match to the Cα chemical shift calculated by Siemons et al.[32] For S31N, there are also two possible conformers for the residues I32 and I39, but this time they are (t, g_p) and (t, t), with (t, g_p) matching the Cα shift according to Siemons et al.[32] The unusual Cα chemical shifts of I32 and I39 of S31N $M2_{18-60}$ at 61.4 and 60.4 ppm, respectively, can therefore be explained by the (t, g_p) rotamer, consistent with the TREDOR data.[27]

The Biological and Structural Relevance of Protein Symmetry Breaking

Biological systems abide by the rule of economy in material and energy. As a consequence, it is unsurprising that molecular structures like proteins, and larger assemblies such as enzymes, are often constructed from identical building blocks, thereby reducing the required genetic material. Identical monomers, when bound together to create a larger complex, usually adopt symmetrical oligomeric conformations, which results from energy minimization within each monomer, as well as minimization at the interfaces between monomers. However, biological molecules often deviate from perfect symmetry to fulfill specific functions. In this case, asymmetry provides characteristic dynamic, assembly, and recognition properties to the oligomer.[34] There are many examples of dimeric enzymes that can allosterically switch between symmetrical states in response to external chemical stimuli.[35] In other cases, asymmetry appears to be an intrinsic property of the oligomer.[36]

Helix-helix interfaces themselves typically contain heterotypic interactions, as is particularly clear for salt bridges. Thus, the stabilizing elements observed in either symmetric or asymmetric assemblies are similar, and can be compared to the vast knowledge regarding heterotypic proteins that interact in the membrane.[37] Indeed, from a physics perspective, spontaneous symmetry breaking is well-known to occur for the state of a system, while obeying symmetric physical laws.[38] A familiar example is the existence of crystals.

In the case of M2, symmetry breaking might be the result of a steric clash: in a 4-fold symmetric state, the large W41 sidechain that points towards the center of the tetramer stands in the way of a compact tetramer. A compact tetramer would optimally hide the hydrated and more polar protein core from the hydrophobic environment of the membrane, and thus be favored. Such a steric clash can be relieved by a small translation of each helix of the tetramer relative to its neighbors. The reduced clash must then be balanced against an expected increase in hydrophobic mismatch within the lipid bilayer. Alternatively, clash could be relieved via changes in the side-chain rotameric states of some of the helices, as seen in the structure 2N70. These simple arguments illustrate how symmetry breaking in a minimalistic tetramer can be explained with energetic arguments to result in a more compact structure, as compared to what is possible with 4-fold symmetry.

Conclusions

We measured spectra of S31N M2 across a range of lipid compositions and using both high and low ratios of solvating lipids. We found the overall dimer-of-dimers structure of S31N M2 to be remarkably stable to these changes. By contrast, a

change to a variant of the protein (Columbia) that substitutes amphipathic helix residues, was found to result in loss of the characteristic peaks that indicate stable His-His hydrogen bonding. We further investigated the structural explanation for unusual isoleucine chemical shifts by measuring internuclear distances, finding that a change of rotameric state occurs, rather than a drastic change in backbone secondary structure. This highlights isoleucine as a challenging case for chemical shift-based backbone secondary structure prediction. The persistence of the dimer-of-dimers structure in different lipid environments solidifies our understanding of the structural template of the apo protein, which we expect to be considered in the development of new antiviral drugs.

Supporting Information Summary

The authors have cited additional references within the Supporting Information.[22,23,25,33,39]

Acknowledgements

We thank Melanie Wegstroth for technical help with M2 sample preparation. This work was supported by the Deutsche Forschungsgemeinschaft through the Emmy Noether Program grant AN1316/1-1 (L.B.A.) and by the Max Planck Society. Open Access funding enabled and organized by Projekt DEAL.

Conflict of Interests

The authors declare no conflict of interest.

Data Availability Statement

The data that support the findings of this study are available in the supplementary material of this article.

Keywords: Influenza · Lipids · M2 · Rotamers · Solid-state NMR · Magic-angle spinning

[1] T. A. Cross, D. T. Murray, A. Watts, *Eur. Biophys. J.* **2013**, *42*, 731–755.
[2] L. Martinez-Gil, I. Mingarro, *Viruses* **2015**, *7*, 3462–3482.
[3] T. Raschle, P. Rios Flores, C. Opitz, D. J. Müller, S. Hiller, *Angew. Chem. Int. Ed.* **2016**, *55*, 5952–5955.
[4] a) J. Hu, R. Fu, K. Nishimura, L. Zhang, H. X. Zhou, D. D. Busath, V. Vijayvergiya, T. A. Cross, *Proc. Natl. Acad. Sci. U. S. A.* **2006**, *103*, 6865-6870; b) C. Wang, R. A. Lamb, L. H. Pinto, *Biophys. J.* **1995**, *69*, 1363–1371.
[5] Y. Tang, F. Zaitseva, R. A. Lamb, L. H. Pinto, *J. Biol. Chem.* **2002**, *277*, 39880–39886.
[6] a) A. Krumbholz, M. Schmidtke, S. Bergmann, S. Motzke, K. Bauer, J. Stech, R. Dürrwald, P. Wutzler, R. Zell, *J. Gen. Virol.* **2009**, *90*, 900–908; b) H. Suzuki, R. Saito, H. Masuda, H. Oshitani, M. Sato, I. Sato, *J. Infect. Chemother.* **2003**, *9*, 195–200.
[7] a) T. A. Cross, M. Sharma, M. Yi, H. X. Zhou, *Trends Biochem. Sci.* **2011**, *36*, 117–125; b) R. Linser, M. Dasari, M. Hiller, V. Higman, U. Fink, J. M. Lopez Del Amo, S. Markovic, L. Handel, B. Kessler, P. Schmieder, D. Oesterhelt, H. Oschkinat, B. Reif, *Angew. Chem. Int. Ed.* **2011**, *50*, 4508–4512; c) A. McDermott, *Annual Review of Biophysics* **2009**, *38*, 385–403; d) K. Xue, K. T. Movellan, X. C. Zhang, E. E. Najbauer, M. C. Forster, S. Becker, L. B. Andreas, *Chem. Sci.* **2021**, *12*, 14332–14342.
[8] a) S. Cady, T. Wang, M. Hong, *J. Am. Chem. Soc.* **2011**, *133*, 11572–11579; b) T. Schubeis, T. Le Marchand, C. Daday, W. Kopec, K. T. Movellan, J. Stanek, T. S. Schwarzer, K. Castiglione, B. L. de Groot, G. Pintacuda, L. B. Andreas, *Proc. Natl. Acad. Sci. U. S. A.* **2020**, *117*, 21014–21021.
[9] D. T. Murray, I. Hung, T. A. Cross, *J. Magn. Reson.* **2014**, *240*, 34–44.
[10] N. Thakur, A. P. Ray, L. Sharp, B. Jin, A. Duong, N. G. Pour, S. Obeng, A. V. Wijesekara, Z. G. Gao, C. R. McCurdy, K. A. Jacobson, E. Lyman, M. T. Eddy, *Nat. Commun.* **2023**, *14*, 1–13.
[11] a) J. K. Williams, D. Tietze, J. Wang, Y. Wu, W. F. Degrado, M. Hong, *J. Am. Chem. Soc.* **2013**, *135*, 9885–9897; b) K. Tekwani Movellan, M. Wegstroth, K. Overkamp, A. Leonov, S. Becker, L. B. Andreas, *J. Struct. Biol.: X* **2023**, *8*, 100090.
[12] L. H. Pinto, L. J. Holsinger, R. A. Lamb, *Cell* **1992**, *69*, 517–528.
[13] J. S. Rossman, R. A. Lamb, *Virology* **2011**, *411*, 229–236.
[14] a) L. B. Andreas, A. B. Barnes, B. Corzilius, J. J. Chou, E. A. Miller, M. Caporini, M. Rosay, R. G. Griffin, *Biochemistry* **2013**, *52*, 2774–2782; b) S. D. Cady, K. Schmidt-Rohr, J. Wang, C. S. Soto, W. F. DeGrado, M. Hong, *Nature* **2010**, *463*, 689–U127; c) A. L. Stouffer, R. Acharya, D. Salom, A. S. Levine, L. Di Costanzo, C. S. Soto, V. Tereshko, V. Nanda, S. Stayrook, W. F. DeGrado, *Nature* **2008**, *451*, 596–599.
[15] J. S. Rossman, X. Jing, G. P. Leser, R. A. Lamb, *Cell* **2010**, *142*, 902–913.
[16] a) B. J. Chen, G. P. Leser, D. Jackson, R. A. Lamb, *J. Virol.* **2008**, *82*, 10059–10070; b) R. A. Lamb, S. L. Zebedee, C. D. Richardson, *Cell* **1985**, *40*, 627-633.
[17] C. Ma, L. Polishchuk, Y. Ohigashi, L. Stouffer, A. Schon, E. Magavern, X. Jing, J. D. Lear, E. Freire, R. Lamb, W. F. DeGrado, L. H. Pinto, *Proc. Natl. Acad. Sci. U. S. A.* **2009**, *106*, 12283–12288.
[18] M. Sharma, M. Yi, H. Dong, H. Qin, E. Peterson, D. D. Busath, H. X. Zhou, T. A. Cross, *Science* **2010**, *330*, 509–512.
[19] L. B. Andreas, M. T. Eddy, R. M. Pielak, J. Chou, R. G. Griffin, *J. Am. Chem. Soc.* **2010**, *132*, 10958–10960.
[20] J. L. Thomaston, A. Konstantinidi, L. Liu, G. Lambrinidis, J. Tan, M. Caffrey, J. Wang, W. F. Degrado, A. Kolocouris, *Biochemistry* **2020**, *59*, 627–634.
[21] a) J. L. Thomaston, M. Alfonso-Prieto, R. A. Woldeyes, J. S. Fraser, M. L. Klein, G. Fiorin, W. F. DeGrado, *Proc. Natl. Acad. Sci. U. S. A.* **2015**, *112*, 14260–14265; b) J. L. Thomaston, Y. Wu, N. Polizzi, L. Liu, J. Wang, W. F. DeGrado, *J. Am. Chem. Soc.* **2019**, *141*, 11481–11488.
[22] A. K. Wright, J. Paulino, T. A. Cross, *J. Am. Chem. Soc.* **2022**, *144*, 2137–2148.
[23] T. V. Can, M. Sharma, I. Hung, P. L. Gorkov, W. W. Brey, T. A. Cross, *J. Am. Chem. Soc.* **2012**, *134*, 9022–9025.
[24] M. Hishida, K. Tanaka, *Phys. Rev. Lett.* **2011**, *106*, 158102.
[25] J. R. Schnell, J. J. Chou, *Nature* **2008**, *451*, 591–595.
[26] a) V. S. Mandala, J. K. Williams, M. Hong, *Annual Review of Biophysics* **2018**, *47*, 201–222; b) T. Schubeis, T. Le Marchand, L. B. Andreas, G. Pintacuda, *J. Magn. Reson.* **2018**, *287*, 140–152.
[27] L. B. Andreas, M. Reese, M. T. Eddy, V. Gelev, Q. Zhe Ni, E. A. Miller, L. Emsley, G. Pintacuda, J. J. Chou, R. G. Griffin, *J. Am. Chem. Soc.* **2015**, *137*, 14877–14886.
[28] K. T. Movellan, M. Wegstroth, K. Overkamp, A. Leonov, S. Becker, L. B. Andreas, *J. Am. Chem. Soc.* **2020**, *142*, 2704–2708.
[29] M. Callon, A. A. Malär, S. Pfister, V. Římal, M. E. Weber, T. Wiegand, J. Zehnder, M. Chávez, R. Cadalbert, R. Deb, A. Däpp, M. L. Fogeron, A. Hunkeler, L. Lecoq, A. Torosyan, D. Zyla, R. Glockshuber, S. Jonas, M. Nassal, M. Ernst, A. Böckmann, B. H. Meier, *J. Biomol. NMR* **2021**, *75*, 255–272.
[30] P. T. Ivanova, D. S. Myers, S. B. Milne, J. L. McClaren, P. G. Thomas, H. A. Brown, *ACS Infect. Dis.* **2016**, *1*, 435–442.
[31] X. C. Zhang, M. C. Forster, E. Nimerovsky, K. T. Movellan, L. B. Andreas, *J. Phys. Chem. A* **2021**, *125*, 754–769.
[32] L. Siemons, B. Uluca-Yazgi, R. B. Pritchard, S. McCarthy, H. Heise, D. F. Hansen, *Chem. Commun.* **2019**, *55*, 14107–14110.
[33] Y. Shen, A. Bax, *J. Biomol. NMR* **2013**, *56*, 227–241.
[34] J. H. Brown, *Protein Sci.* **2006**, *15*, 1–13.
[35] a) J. Monod, J.-P. Changeux, F. Jacob, *J. Mol. Biol.* **1963**, *6*, 306–329; b) J. Monod, J. Wyman, J.-P. Changeux, *J. Mol. Biol.* **1965**, *12*, 88–118.
[36] F. Seydoux, O. P. Malhotra, S. A. Bernhard, G. Stark, *CRC Crit. Rev. Biochem.* **1974**, *2*, 227–257.
[37] a) D. Steindorf, D. Schneider, *Biochim. Biophys. Acta (BBA) – Biomembr.* **2017**, *1859*, 245–256; b) B. R. Sahoo, A. Ramamoorthy, *Biophys. Chem.*

2023, *301*, 107092; c) A. García-Recio, G. Navarro, R. Franco, M. Olivella, R. Guixà-González, A. Cordomí, *Bioinformatics* **2020**, *36*, 3271–3272.
[38] D. J. Gross, *Proc. Natl. Acad. Sci.* **1996**, *93*, 14256–14259.
[39] a) Y. A. Andreev, S. A. Kozlov, A. A. Vassilevski, E. V. Grishin, *Anal. Biochem.* **2010**, *407*, 144–146; b) A. E. Bennett, J. H. Ok, R. G. Griffin, S. Vega, *J. Chem. Phys.* **1992**, *96*, 8624–8627; c) A. E. Bennett, C. M. Rienstra, M. Auger, K. V. Lakshmi, R. G. Griffin, *J. Chem. Phys.* **1995**, *103*, 6951–6958; d) T. Gullion, S. Vega, *Chem. Phys. Lett.* **1992**, *194*, 423–428; e) R. Paschke, S. Mohr, S. Lange, A. Lange, J. Kozuch, *Angew. Chem. Int. Ed* **2023**, *62*, e202309069; f) O. Weintraub, S. Vega, C. Hoelger, H. H. Limbach, *J. Magn. Reson., Ser. A* **1994**, *109*, 14–25; g) E. E. Najbauer, L. B. Andreas, *J. Magn. Reson.* **2019**, *305*, 1–4; h) H. Geen, R. Freeman, *J. Magn. Reson. (1969)* **1991**, *93*, 93–141.

Manuscript received: August 25, 2024
Accepted manuscript online: November 7, 2024
Version of record online: December 4, 2024